Article

Current Biology

Ciliary flows in corals ventilate target areas of high photosynthetic oxygen production

Graphical abstract

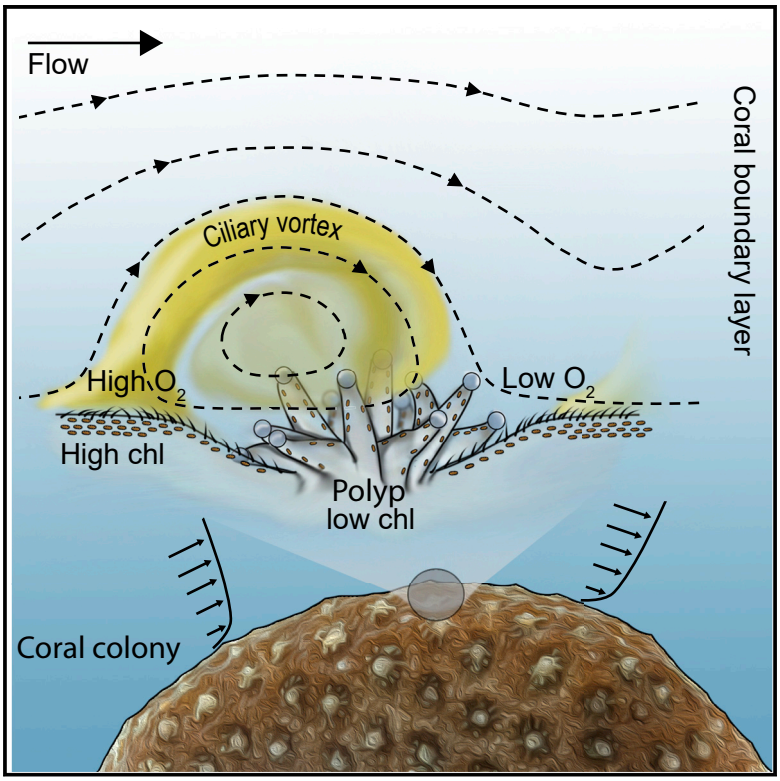

Highlights

- Chlorophyll in the coral tissue is higher in the coenosarc and lower in the mouth
- O_2 in the DBL shows an inverse distribution from that of Chl*a*
- Ciliary vortices at the coral surface carry O_2 from areas of high to low production
- Cilia-generated vortices may help minimize oxidative stress inside the coral tissue

Authors

Cesar O. Pacherres, Soeren Ahmerkamp, Klaus Koren, Claudio Richter, Moritz Holtappels

Correspondence

cesar.pacherres@bio.ku.dk (C.O.P.), sahmerka@mpi-bremen.de (S.A.)

In brief

Pacherres, Ahmerkamp et al. present simultaneous measurements of flow and O_2 in the coral boundary layer along with Chl*a* content in the tissue beneath, showing a patchiness in the O_2 distribution that is shifted away from O_2-production zones by ciliary vortices; a mechanism that might help corals mitigate potential oxidative damage and bleaching.

Pacherres et al., 2022, Current Biology *32*, 1–9
October 10, 2022 © 2022 The Author(s). Published by Elsevier Inc.
https://doi.org/10.1016/j.cub.2022.07.071

CellPress

Please cite this article in press as: Pacherres et al., Ciliary flows in corals ventilate target areas of high photosynthetic oxygen production, Current Biology (2022), https://doi.org/10.1016/j.cub.2022.07.071

Current Biology

CellPress
OPEN ACCESS

Article

Ciliary flows in corals ventilate target areas of high photosynthetic oxygen production

Cesar O. Pacherres,[1,2,3,7,8,10,*] Soeren Ahmerkamp,[4,5,7,9,*] Klaus Koren,[6] Claudio Richter,[1,2] and Moritz Holtappels[1,5]
[1]Alfred Wegener Institute, Helmholtz Center for Polar and Marine Research, 27568 Bremerhaven, Germany
[2]Department of Biology and Chemistry, University of Bremen, 28359 Bremen, Germany
[3]Marine Biological Section, Department of Biology, University of Copenhagen, 3000 Helsingør, Denmark
[4]Max Planck Institute for Marine Microbiology, 28359 Bremen, Germany
[5]MARUM - Center for Marine Environmental Sciences, University of Bremen, 28359 Bremen, Germany
[6]Center for Water Technology, Section for Microbiology, Department of Biology, Aarhus University, 8000 Aarhus, Denmark
[7]These authors contributed equally
[8]Twitter: @pacherres_co
[9]Twitter: @SoerenAhm
[10]Lead contact
*Correspondence: cesar.pacherres@bio.ku.dk (C.O.P.), sahmerka@mpi-bremen.de (S.A.)
https://doi.org/10.1016/j.cub.2022.07.071

SUMMARY

Most tropical corals live in symbiosis with Symbiodiniaceae algae whose photosynthetic production of oxygen (O_2) may lead to excess O_2 in the diffusive boundary layer (DBL) above the coral surface. When flow is low, cilia-induced mixing of the coral DBL is vital to remove excess O_2 and prevent oxidative stress that may lead to coral bleaching and mortality. Here, we combined particle image velocimetry using O_2-sensitive nanoparticles (sensPIV) with chlorophyll (Chl*a*)-sensitive hyperspectral imaging to visualize the microscale distribution and dynamics of ciliary flows and O_2 in the coral DBL in relation to the distribution of Symbiodiniaceae Chl*a* in the tissue of the reef building coral, *Porites lutea*. Curiously, we found an inverse relation between O_2 in the DBL and Chl*a* in the underlying tissue, with patches of high O_2 in the DBL above low Chl*a* in the underlying tissue surrounding the polyp mouth areas and pockets of low O_2 concentrations in the DBL above high Chl*a* in the coenosarc tissue connecting neighboring polyps. The spatial segregation of Chl*a* and O_2 is related to ciliary-induced flows, causing a lateral redistribution of O_2 in the DBL. In a 2D transport-reaction model of the coral DBL, we show that the enhanced O_2 transport allocates parts of the O_2 surplus to areas containing less chl*a*, which minimizes oxidative stress. Cilary flows thus confer a spatially complex mass transfer in the coral DBL, which may play an important role in mitigating oxidative stress and bleaching in corals.

INTRODUCTION

Coral reefs are among the most diverse and economically important ecosystems on the planet.[1] Despite their importance as ecosystem engineers, the corals providing the foundation of today's reefs are threatened by a multitude of anthropogenic changes acting on many spatial and temporal scales.[2,3] Nutrification of coastal areas in the wake of deforestation, increased terrestrial run-off over the last century,[4,5] and overfishing, dating back to the origin of human expansion,[6] have caused coral-algal phase shifts.[7] Global effects such as ocean acidification, deoxygenation, and warming have caused severe mass bleaching and mortality of corals[8–10] contributing to the demise of corals in all reef provinces over the last decades.[11,12] However, although the importance of corals and their threats can be assessed on a broad scale (colonies and reefs), it is the individual coral polyp (usually mm in size) and its symbionts that are directly responding to anthropogenic disturbances.[13] Hence, our ability to estimate the response of coral reefs to environmental stressors requires a deep understanding of polyp-scale physiology and the manner in which it reacts to disturbances.

Tropical scleractinian corals live in symbiosis with dinoflagellate algae (Symbiodiniaceae), an association that allows them to recycle essential elements and thrive in nutrient-poor waters.[14,15] Within the coral tissue, symbiont distribution can be highly heterogeneous, with densities dependent on tissue structure, light, and nutrient availability.[16–18] Among the Symbiodiniaceae, chlorophyll concentrations can be highly variable, since the coral holobiont can adapt to reduced light by increasing the symbiont and/or chlorophyll densities in order to optimize light harvesting.[19,20] Symbiont and pigment densities, together with the tissue's optical properties, generate physiological microniches—suggested to play the role of refugia for minor symbiont populations—which might be important for the coral's response to stress.[13,21] Therefore, understanding where the symbionts are located along and across the coral tissue becomes highly relevant, although *in vivo* studies of Symbiodiniaceae distribution at μ-metric resolutions are still scarce.

This is an open access article under the CC BY license (http://creativecommons.org/licenses/by/4.0/).

Please cite this article in press as: Pacherres et al., Ciliary flows in corals ventilate target areas of high photosynthetic oxygen production, Current Biology (2022), https://doi.org/10.1016/j.cub.2022.07.071

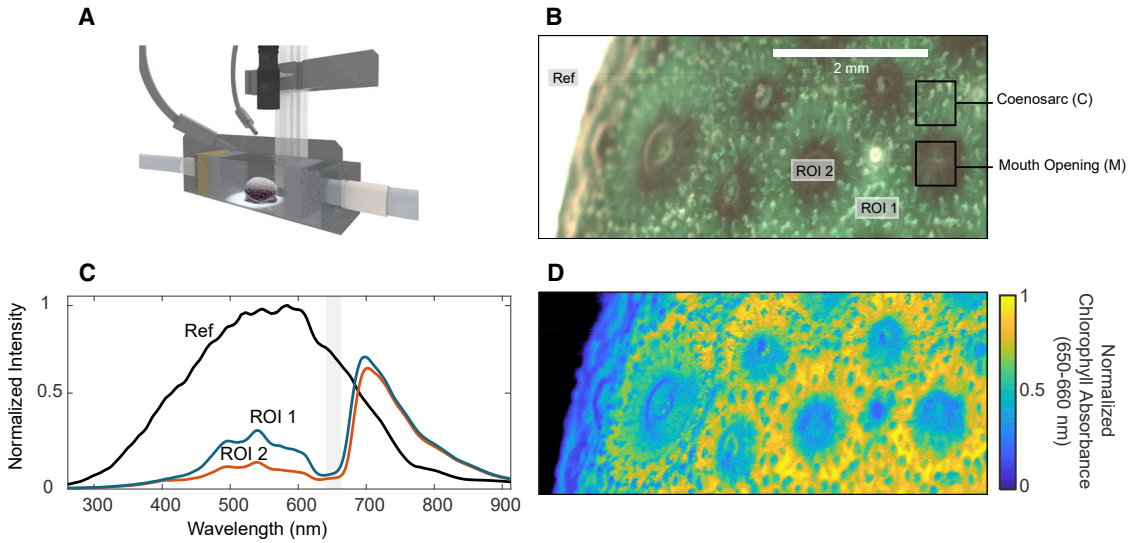

Figure 1. Hyperspectral imaging of Symbiodiniaceae Chl*a* distribution in *Porites lutea*

(A) Experimental setup showing the arrangement of the coral inside the flow-through chamber with the hyperspectral camera and lens on top which were moved horizontally using a linear motor.

(B) Processed image of the coral surface showing the regions of interest (ROIs) and the external reference area. Coenosarc (C) and mouth (M) opening are marked. See also Figure S1.

(C) Normalized light intensities at the ROIs and reference shown in (B). The gray bar indicates the wavelength that were used for absorbance in (D).

(D) Map of the Chl*a* concentrations inside the coral tissue derived from normalized chlorophyll absorbance.

The relationship between the coral and its Symbiodiniaceae symbionts is highly complex. Although the coral consumes most of the O_2 produced by its symbionts,[22] the surplus diffuses out of the tissue into the coral-water interface—the diffusive boundary layer (DBL).[23] Diffusion acts as a bottleneck for solute exchange and indirectly controls the coral's physiology[24,25] and stress response.[26,27] In the coral *Favia* sp., spatial variations in O_2 and CO_2 within a single polyp were attributed to coral morphology causing μ-metric variations in the thickness of the DBL and differences in the light field.[28] Similarly higher photosynthetic rates were found in the middle parts of the corallite, tentacles, and tissue surrounding the mouth of *Galaxea fascicularis*, whereas the wall of the corallite and the coenosarc showed lower photosynthetic rates[29] (see also Figure S1 for details on coral structure). This heterogeneity was attributed to differences in symbiont distribution, localized higher photosynthetic activity in response to increased metabolic demand and local supply of solutes through the DBL,[29] but concurrent assessments of symbiont distribution and O_2 are so far lacking. The response of corals to environmental stress, and subsequent bleaching, has also been partly attributed to the DBL controlling the exchange of O_2 and solutes between the coral and the water column.[30,31] Although O_2 exchange in the coral tissue and DBL has long been considered passive by means of diffusion,[24,32] more recent work has shown the importance of ciliary currents enhancing the effective diffusivity at the coral surface.[33,34] Ciliary action was shown to lower excessive O_2 concentrations at the coral surface serving predominantly as a homeostatic control mechanism in coral stress response.

The heterogeneities in symbiont distribution, photosynthesis, host activity (respiration), and ciliary flows are therefore likely to result in a complex patterning of the O_2 microenvironment of the coral, with differential O_2 accumulation and/or consumption and contrasting cellular responses to O_2 levels. Although O_2 is essential for all aerobic organisms, excess O_2 can be detrimental for photoautotrophs[35,36] especially under high temperatures.[37] Since the photosynthetic apparatus of the symbiont—Rubisco Form II—has a higher affinity to O_2 over CO_2, the excess of the former causes photorespiration and the production of O_2 radicals.[38] This not only entails higher metabolic costs[39] but also may cause cellular damage and, ultimately, coral bleaching.[40–42] Moreover, the documented high spatial variability of photosynthetic activity[24,28,29] raises the question of how corals deal with the potential negative impacts of localized hyperoxia.

Therefore, understanding the O_2 dynamics along and across the different compartments of the coral, i.e., DBL, tissue, and symbionts, is of paramount importance since it has a direct influence on its health, performance, and ability to respond to its environment. Here, we provide the first simultaneous assessment of the microscale flow field and two-dimensional O_2 distribution in the coral boundary layer under controlled ambient illumination and currents, along with a mapping of Symbiodiniaceae Chl*a* concentrations in the underlying coral tissue. We aim to characterize the Chl*a* distribution inside the coral tissue and relate it with the O_2 and flow dynamics at the coral surface, examining the role of ciliary flows in the transport of O_2 away from the tissue surface.

RESULTS AND DISCUSSION

Chl*a* concentrations in the coral tissue

Using hyperspectral imaging technology,[43] we analyzed the areal Chl*a* distribution in the tissue of the coral *Porites lutea* at a sub-millimeter scale. We observed higher normalized absorbance of 0.8 in the coenosarc, indicating high Chl*a* concentration (Figure 1B, ROI 1; Figure 1D, yellow areas). In contrast,

Please cite this article in press as: Pacherres et al., Ciliary flows in corals ventilate target areas of high photosynthetic oxygen production, Current Biology (2022), https://doi.org/10.1016/j.cub.2022.07.071

CellPress
OPEN ACCESS

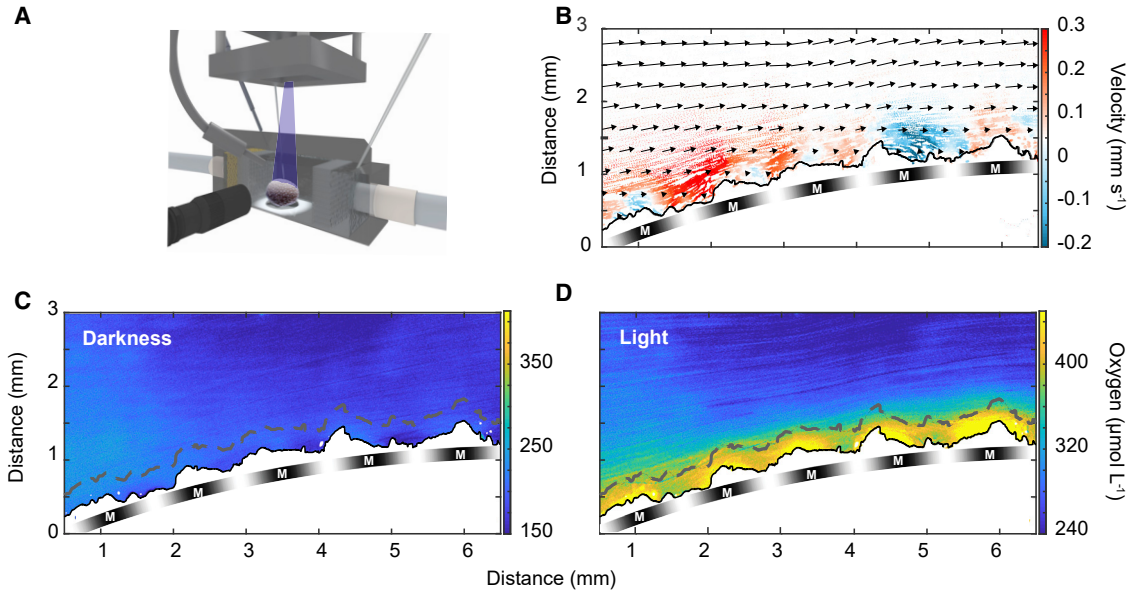

Figure 2. O_2 and flow dynamics in the DBL of *Porites lutea* measured simultaneously using sensPIV

(A) Experimental setup showing the coral colony inside the flow-through chamber with the light sheet illumination from above and imaging from the side. See also Pacherres et al.[33]

(B) Combined particle image velocimetry (PIV) and particle tracking velocimetry (PTV) of sensPIV particles under light conditions. Arrows indicate the temporally averaged water flow direction on top of the coral surface. Colored dots represent single tracked particles, and the color indicates their vertical velocity. Red and blue depict upward and downward flow of particles, respectively, indicating the position of vortices. See also Figure S3 and Table S1.

(C and D) O_2 concentrations (extracted from the sensPIV signal) in the DBL of the coral exposed to (C) 1 h of darkness and (D) 5 min of light (after acquisition of images under dark condition).The solid black line shows the profile of the coral surface; the dashed line the distance of 0.3 mm from the coral surface. The black and white strip beneath the coral surface indicates areas of high and low chlorophyll near coenosarc (white) and mouth (M) openings (black), respectively. See also Figures S1 and S2. Flow speed of water was 300 µm s^{-1} measured at a distance of 2 mm from the coral surface.

normalized absorbance was 0.3 at the mouth openings, indicating low Chl*a* concentration (Figure 1B, ROI 2; Figure 1D, blue areas). As the polyps of *Porites* tend to remain partially retracted during the day[44] in order to enhance planar density and photosynthetic performance of its symbionts,[45,46] it is no surprise that the coenosarc contains higher Chl*a* concentrations than the area surrounding the mouth. The quantification and distribution of Chl*a* densities in the thin veneer of tissue covering the complex coral skeleton has only recently been made possible by the application of high-resolution optical techniques[47,48] requiring extensive sample preparation[48] or the short-term removal of culturing water.[47] Here, images were taken in a flow-through chamber, without disturbing the coral. We expected the spatial heterogeneities in symbiont distribution to be reflected also in the O_2 DBL's landscape, as the differential diffusion of photosynthesis-derived O_2 has been shown to lead to a patchy distribution of O_2 diffusing to the surface of the coral,[49] with highest values over the coenosarc and lowest values over the polyp mouths.

Flow field and O_2 concentrations at the coral surface

In order to relate the heterogeneous Chl*a* distribution inside the tissue with the O_2 dynamics at the DBL, we used particle image velocimetry (PIV) using O_2-sensitive nanoparticles in an image velocimetry system (sensPIV)[50] (Figure 2A). We observed a heterogeneous O_2 distribution along the coral surface. However, areas of high O_2 concentrations (hotspots) coincided with areas of low Chl*a* concentration over the mouth openings of the coral polyps, whereas areas of lower O_2 concentrations coincided with areas of high Chl*a* concentration over the coenosarc (Figure 2D). The opposed patchiness suggests the superposition of two independent processes: passive diffusion of O_2 from the sites of production (symbionts) and active transport of water by ciliary currents, as outlined below.

Under the flow conditions of our experiments (300 and 1,500 µm s^{-1}), cilia on the surface of the coral generated vortical currents (Figure 2B). At high ambient flow speeds (1,500 µm s^{-1}), the average height and width of the vortices were 300 ± 55 µm and 1,500 ± 230 µm, respectively. At low ambient flow speeds (300 µm s^{-1}), the corresponding values were 500 ± 50 µm and 1,500 ± 220 µm, respectively (Figure S2). Within the vortices, the vertical flow velocities reached up to 300 µm s^{-1} and −200 µm s^{-1} (Figure 2B), in line with previous reports.[33,34] The vortices' structure was similar to those found in Pacherres et al.[33] with the upward flow of the vortex facing toward the ambient current, whereas the downward flow was located leeward, suggesting cilia beating against the ambient current (Figure S3). The upward flank of the vortices transported water from the coral polyp periphery aloft (red areas, Figure 2B), whereas the downward flank was situated somewhat leeward of the polyp mouth opening (blue areas, Figure 2B). As a result, the main part of the vortices was situated on top of the mouth opening. In darkness, we found slightly lowered O_2 concentrations in the downwelling areas suggesting respiration (Figure 2C)

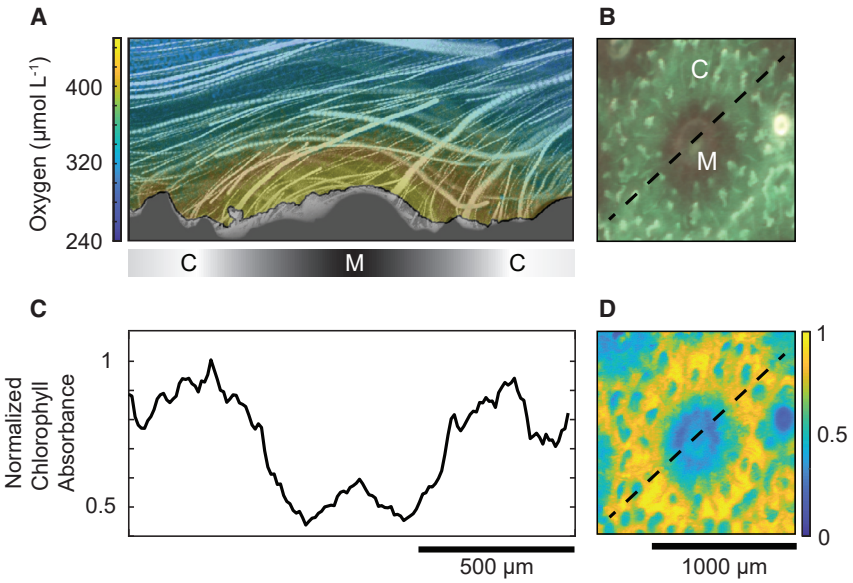

Figure 3. Combined flow dynamics, surface O_2, and internal Chl*a* of a single polyp of *Porites lutea*

(A and B) Flow dynamics (depicted by the particle trajectories) and O_2 concentration (color map) extracted from the SensPIV results along the dashed line shown in (B). Black and white panel below indicates different regions of the coral: coenosarc (C) (white) and mouth (M) opening (black) (as in Figure 2). See also Figure S1.

(C and D) Normalized Chl*a* absorption (used as a proxy for Chl*a* concentrations) along the dashed line shown in (D). Please notice that O_2 distribution and chlorophyll distribution are not from the same locations but are picked as representative examples. Scale bars are applicable for the respective vertical panels.

with similar velocity magnitudes inside the vortex area (Table S1). In the light, we found high O_2 concentrations near the coral surface, with highest values over the mouths and lower values in the periphery (Figure 2D).

Combining O_2 at the DBL and tissue Chl*a*

The inverse relation between O_2 and Chl*a* distributions is in conflict with the current paradigm of an exclusively diffusive transport of O_2, which would predict a positive relation between Chl*a* and O_2. We found the opposite, a redistribution of O_2 by cilia-induced vortical currents dominating O_2 transport in *Porites*. The vortices were located above the Chl*a*-poor areas, with their upward flow extending into the adjacent Chl*a*-rich areas (Figure 3). This allows O_2 to be transported laterally from the main production site into the vortex, which itself extends vertically as a bulged interface into the ambient water with lower O_2. As a result, O_2 accumulation in the Chl*a*-rich tissue is alleviated, and at the same time, the high O_2 concentration in the vortex increases the concentration gradient toward the ambient water and thus the diffusive flux.

Previous microsensor studies of O_2 concentrations at the surface of *Favia* sp. found peaks of gross photosynthetic production in the coenosarc[24,28] and large variations in the O_2 concentrations in the water column above the mouth.[28] On the other hand, *Galaxea fascicularis* showed an order of magnitude increase in gross O_2 production over the polyp mouth compared with the coenosarc.[29] Although our observations are in line with some of these early studies, it is important to acknowledge that corals exhibit a high plasticity of forms, tissue properties, symbiont distribution, and Chl*a* content (see introduction), all of which influence the diffusion of solutes along, across, and outside of the tissue. Therefore, further research on the linkages between the different coral compartments, using other coral species, will be needed in order to better understand how coral form and functions are related and the way in which they might optimize coral respond to stressors.

Simulations of the boundary layer dynamics of *P. lutea*

To investigate the relation between tissue Chl*a* and the diffusive and advective fluxes of photosynthetic O_2, we simulated the effects of diffusion and ciliary flow along the coral surface by means of a simplified planar two-layer model. The lower layer has a thickness of 100 µm, representing the tissue of *P. lutea* in which the Symbiodiniaceae are located, and transport is limited to diffusion (dotted line in Figure 4A). The heterogeneously distributed symbionts produce O_2 at a constant rate, assuming constant light regime and no oxidative stress. The layer above represents the water column in which the cilia stir the boundary layer under flow conditions. The ciliary flow is driven by a moving boundary with horizontal velocity components that oscillate in both directions along the surface at an amplitude (maximum ciliary flow) that was adjusted to c_{vel} = 150 µm s^{-1}, similar to previous measurements.[34] The undisturbed flow velocity in the simulation was set to 300 µm s^{-1}, similar to the measurements.

The interaction of the flow field and the beating of cilia leads to vertical flow speeds of 80–100 µm s^{-1}, which are slightly lower than the maximum vertical speeds from the experiments (up to 300 µm, Figure 1B) and the velocities seen in the upward zones of the vortices in Shapiro et al.[34] At the coral surface, the opposing horizontal velocities lead to the formation of two stagnation points: at one stagnation point, the currents converge, driving the flow aloft into the boundary layer; at the other, the currents diverge where the downward flow returns to the coral surface and is deflected sideways. The upward and downward flows drive the vortices lining the surface of the coral. The horizontal extent of the vortices is largely determined by the boundary conditions, i.e., the wavelength of the oscillating boundary, which was adjusted to δ = 1,200 µm, similar to the average size of the calyx of the coral (see details of calyx size in Figure 3B). The specific shape of the vortices leads to two distinct regions within the coral boundary layer, which are determined by the location of the stagnation points along the surface of the coral (Figure 4A, red dots and dashed line). The first region (Figure 4A, inserted panel: R1) is the vortex proper, where streamlines are closed, indicating no advective exchange with the surrounding water. The second region (Figure 4A, inserted panel: R2) is

Please cite this article in press as: Pacherres et al., Ciliary flows in corals ventilate target areas of high photosynthetic oxygen production, Current Biology (2022), https://doi.org/10.1016/j.cub.2022.07.071

CellPress
OPEN ACCESS

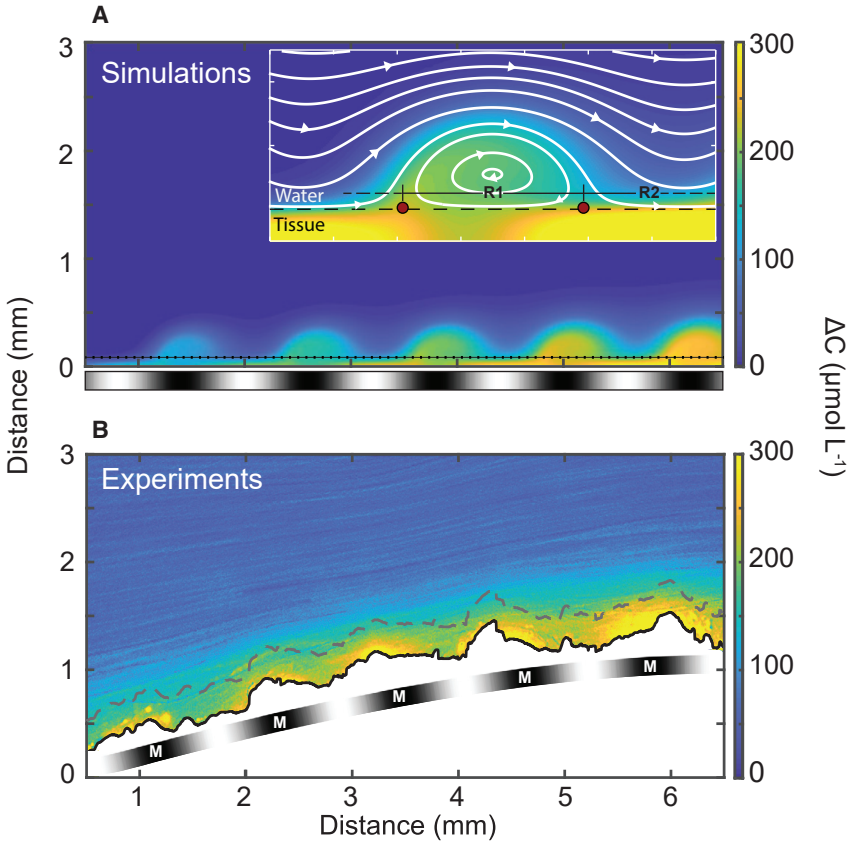

Figure 4. Simulation and experimental results of the flow and O_2 dynamics of the coral DBL

(A) Model results of the O_2 concentration above ambient inside the DBL of the coral under the same flow speed of water as in the experiments. Inserted panel represents the O_2 and flow distribution of a magnified vortex, and red dots depict the stagnation points and the distinct regions, R1 and R2, along the surface and coral DBL, respectively (see text).

(B) Experimental results of the O_2 concentration differences between light and darkness (180 and 0 μmol quanta m^{-2} s^{-1}). Black and white stripes as in Figures 2 and 3.

characterized by a strong flow lining the periphery of the vortex enhancing the concentration gradient and diffusive exchange with the tissue.

In the simulations, O_2 produced diffuses from the coral tissue in proportion to the observed Chl*a* distribution (Figure 2D). For simplicity, the heterogeneity of O_2 production is simulated by a sinusoidal curve whose spatial extent was adjusted to match the experimentally obtained results: highest O_2 production was situated outside the vortex structures, whereas lowest O_2 production was situated underneath the vortex (Figure 3). The produced O_2 diffuses through the tissue before reaching the water column. Along the tissue surface, diffusive exchange fluxes are highest where O_2 gradients between tissue and the ambient water are strongest. The strongest O_2 gradients occur where O_2 is produced at a higher rate and ambient water with low O_2 is directed downward at high velocities (Figure 4A, inserted panel: R2). In contrast, O_2 concentrations within the vortices are elevated, fed by the upward flow of O_2-enriched water from the tissue surface. Although rotating in the vortex, O_2 diffuses across the vortex boundaries into the ambient water so that the downward flow carries less O_2 and can be recharged again (Figure 4A, inserted panel: R1). The simulated O_2 distribution (Figure 4A) exhibits a similar pattern as the measured O_2 distribution (Figure 4B): five distinct vortices reaching up to 500 μm into the flow field become visible where O_2 concentrations are supersaturated. With the model, it is now possible to simulate the interplay of diffusive and advective fluxes, thus resolving the paradox of high O_2 concentrations above low O_2-production sites (Figure 4).

We used the model to test how the location of the vortices above the coral surface affects the O_2 distribution in the DBL and inside the tissue of the coral. O_2 accumulates in the vortices independent of the relative location of vortices and O_2 production sites (Figure 5A). Consequently, the O_2 concentration in the DBL does not reflect the O_2 concentration and production rate in the tissue directly below but is reshaped by the interacting vortical and ambient flow fields. In general, the vortices help to decrease the O_2 concentration in the underlying tissue, as described by Pacherres et al.[33] At ciliary flow conditions similar to the ones in the experiments, we found the spatially averaged O_2 concentration in the tissue to be reduced by 53%, compared with no ciliary flow conditions. However, the efficiency of this reduction depends on the relative location of vortices and hotspots of O_2 production, which has a particular impact on harmful excess O_2 concentrations in the tissue (Figures 5B and 5C). To exemplify this, we calculated the tissue area that is affected by a critical O_2 concentration of more than 300 μmol L^{-1} above ambient levels, a threshold based on Sforza et al.[51] (Figure S5). When vortex location and production hotspots are separated (phase shift: 207°), the area with critical O_2 concentrations is minimized to 20.7% (Figure 5C). When vortex location and production hotspots are aligned (phase shift: 43°), the affected area is nearly doubled to 38% (Video S1). Similar results are found for O_2 concentration thresholds ranging from 200 to 350 μmol L^{-1} above ambient levels (Table S2). It is important to mention that the reallocation of O_2 from the tissue into the vortex does not imply an increased net mass transfer as long as the O_2 production in the coral tissue is independent of the O_2 concentration.

In summary, the simulation shows that the observed O_2 and Chl*a* patterns are not directly connected, but the result of the diffusive flux interacting with the flow field generated by the cilia (Figure 3). The results further indicate that positioning the vortices adjacent to, rather than above, the O_2 production sites selectively enhances the ventilation of O_2-producing symbiont patches, which helps avoid photosynthetic inhibition.

Please cite this article in press as: Pacherres et al., Ciliary flows in corals ventilate target areas of high photosynthetic oxygen production, Current Biology (2022), https://doi.org/10.1016/j.cub.2022.07.071

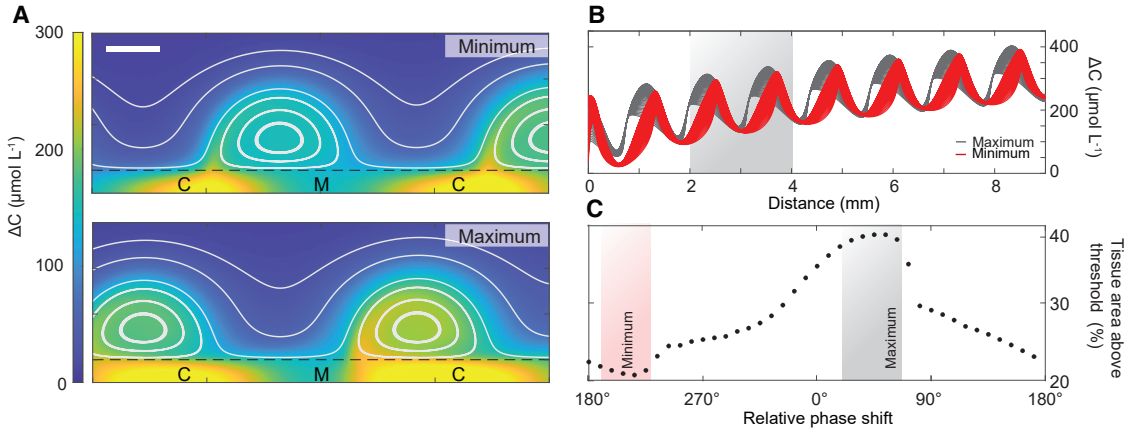

Figure 5. Modeled O_2 concentration above ambient in which the location of the vortices is phase-shifted relative to the peaks of O_2 production

(A) A phase shift of 180° (upper panel) implies that upward directed velocities in the vortex coincide with the peaks of O_2 concentrations, as seen in the experimental results—Figure 4B. A phase shift of 0° (lower panel) implies that the vortex is located above the zones of increased O_2 production. Mouth (M) opening and coenosarc (C). See also Video S1. White bar indicates 500 μm.

(B) Modeled O_2 concentration above ambient along the entire tissue domain, where the gray bar indicates the section shown in (A).

(C) Percentage of tissue area that is above a critical threshold of 300 μmol L^{-1} above ambient O_2 concentration. The red and gray bars indicate the minimum and maximum, respectively. See also Figure S5 and Table S2.

Implications for the coral's response to environmental stress

Ciliary vortices localized adjacent to specific sites of excess O_2 production seem beneficial for the coral in the face of oxidative stress, especially under weak currents, which have been found to exacerbate bleaching.[31,52] It has been suggested that photosynthetic activity by the symbionts may be inhibited by O_2 accumulation through photorespiration and the formation of reactive oxygen species (ROS).[40,53,54] Photorespiration occurs when O_2 is used as substrate instead of CO_2, resulting in the loss of energy,[55] whereas ROS are formed through photoreduction of O_2 and are believed to directly damage the photosystem II of the chloroplast.[37,56] Our results show that the O_2 concentration in the coral tissue can not only be modulated by ciliary flows as such but also depend on the relative location of the vortices with respect to areas of O_2 production, further reducing photosynthetic inhibition by the reallocation of O_2. The generation of this heterogeneous O_2 landscape is of particular importance when taking into consideration that the ability of an organism to adapt to environmental changes, e.g., climate change, highly depends on its life history exposure to short-term and short-scale environmental fluctuations.[44,57,58] It is known that adjacent colonies of the same coral species exposed to the same water temperatures can present different bleaching responses,[59] and more so, different regions within the same colony may show differential bleaching severities.[13] Our findings suggest that microscale heterogeneities in both the internal arrangement of symbionts and the external micro-currents generated by the ciliated surface of the coral represent a composite buffer to mitigate oxidative stress. We postulate that this buffer is an important pre-requisite for coral resistance to bleaching in the face of global warming.

Alternatively, localized vortices might as well be redistributing O_2 to areas where the tissue has less symbionts (and therefore has less local supply of O_2 for the host tissue). During the day, coral symbionts produce an excess of O_2 that by far surpasses the metabolic requirements of a healthy coral.[60] However, measurements of O_2 concentrations inside the gastric cavity of corals have shown extremely low O_2 concentrations even during the day.[61] Whether the coral utilizes ciliary flows as an external transport mechanism linking zones of O_2 production with zones of O_2 consumption would require further exploration.

The observed localized transport mechanism is unlikely to be restricted to O_2 but should also be effective for other solutes. With regard to the seawater carbonate system, vortex transport of DIC and protons might be of significant importance to coral calcification and should be considered in studies of coral physiology under climate change.[8,62] Since coral calcification depends on pH, light, and currents,[63,64] vortex-altered proton transport in the DBL,[33] along with the coral's capacity to upregulate its inner calcifying fluid,[65,66] might help explain the sometimes contradicting, species-specific response of corals to ocean acidification. Research is needed to assess potential vortex effects on coral calcification and coral resilience to ocean acidification.

The ability of corals to enhance mass transport in specific areas (here: the coenosarc) (Figure 2C) might have implications not only in the coral's response to its environment but also in its relationship with bacteria and viruses that inhabit its surface.[67,68] The community of prokaryotic and eukaryotic microbes, viruses, and archaea comprising the coral microbiome is extremely diverse[69] and has been associated not only with diseases[70] but also with the capacity of corals to resist environmental stress by the acquisition of nutrients, defense against pathogens, horizontal gene transfer, etc.[71–73] The ability of cilia to generate chemical microenvironments, such as seen here for the O_2 hotspots, could provide an advantage to certain coral-associated microbes by enhancing the transport of the

Please cite this article in press as: Pacherres et al., Ciliary flows in corals ventilate target areas of high photosynthetic oxygen production, Current Biology (2022), https://doi.org/10.1016/j.cub.2022.07.071

metabolic compounds necessary for their development. Further research will be needed in order to unveil the consequence of the observed microenvironment creation and the repercussions it might have upon coral-microbe relations and coral health.

Conclusions

Altogether, this study demonstrates that the spatial arrangement of local interactions between ciliary flows and physiological processes (photosynthesis) can give rise to local heterogeneities in the chemical landscape and solute exchange. It extends the coral's ability to respond to environmental stressors well into the coral's boundary layer, where the flow field can be shaped according to local needs. A 3D exploration of the coral DBL, taking into consideration the different elements that intervene in its shape and characteristics, can be an important next step to reveal further insights into the complex coral-water interface and better understand the role of the DBL in the coral's relationship with its environment.

STAR★METHODS

Detailed methods are provided in the online version of this paper and include the following:

- KEY RESOURCES TABLE
- RESOURCE AVAILABILITY
  - Lead contact
  - Materials availability
  - Data and code availability
- EXPERIMENTAL MODEL AND SUBJECT DETAILS
- METHOD DETAILS
  - Experimental set-up
  - Hyperspectral imaging
  - SensPIV measurements
- QUANTIFICATION AND STATISTICAL ANALYSIS
  - Model formulation
  - Limitations of the model and topography effects

SUPPLEMENTAL INFORMATION

Supplemental information can be found online at https://doi.org/10.1016/j.cub.2022.07.071.

ACKNOWLEDGMENTS

We thank Esther Lüdtke and Ulrike Holtz for their help with the culturing of the coral colonies, Dr. Arjun Chennu (ZMT) for providing the hyperspectral camera, and Paul Faerber for technical support. This research was conducted in the framework of the PhD project of C.O.P. at the University of Bremen and the Alfred Wegener Institute (AWI). It was supported and financed by FONDECYT, an initiative from the Consejo Nacional de Ciencia, Tecnología e Innovación Tecnológica (CONCYTEC), Perú, Contrato 086-2016-FONDECYT and the AWI (PoF4.6: Marine and Polar Life). MPI-MM Bremen provided logistic and instrumental support. S.A. acknowledges funding from the Max Planck Society (MPG). K.K. acknowledges funding from the Grundfos Foundation and a Sapere Aude grant from the Independent Research Fund Denmark (IRFD): DFF-8048-00057B.

AUTHOR CONTRIBUTIONS

C.O.P., S.A., C.R., and M.H. designed the experiments for this study. C.O.P. conducted all the experiments. C.O.P. and S.A. analyzed the sensPIV and hyperspectral data and generated the result figures. M.H. and S.A. worked on the model and its figures. K.K. created and supplied the sensPIV particles necessary for the oxygen experiments. C.O.P., S.A., K.K., C.R., and M.H. contributed to the interpretation of the collected data and conceived and wrote the manuscript.

DECLARATION OF INTERESTS

The authors declare no competing interests.

Received: March 8, 2022
Revised: July 1, 2022
Accepted: July 26, 2022
Published: August 23, 2022

REFERENCES

1. Costanza, R., de Groot, R., Sutton, P., van der Ploeg, S., Anderson, S.J., Kubiszewski, I., Farber, S., and Turner, R.K. (2014). Changes in the global value of ecosystem services. Glob. Environ. Change *26*, 152–158.
2. Jackson, J.B.C., Kirby, M.X., Berger, W.H., Bjorndal, K.A., Botsford, L.W., Bourque, B.J., Bradbury, R.H., Cooke, R., Erlandson, J., Estes, J.A., et al. (2001). Historical overfishing and the recent collapse of coastal ecosystems. Science *293*, 629–637.
3. van der Zande, R.M., Achlatis, M., Bender-Champ, D., Kubicek, A., Dove, S., and Hoegh-Guldberg, O. (2020). Paradise lost: end-of-century warming and acidification under business-as-usual emissions have severe consequences for symbiotic corals. Glob. Change Biol. *26*, 2203–2219.
4. McCulloch, M., Fallon, S., Wyndham, T., Hendy, E., Lough, J., and Barnes, D. (2003). Coral record of increased sediment flux to the inner Great Barrier Reef since European settlement. Nature *421*, 727–730.
5. Fabricius, K.E. (2005). Effects of terrestrial runoff on the ecology of corals and coral reefs: review and synthesis. Mar. Pollut. Bull. *50*, 125–146.
6. Richter, C., Roa-Quiaoit, H., Jantzen, C., Al-Zibdah, M., and Kochzius, M. (2008). Collapse of a new living species of giant clam in the Red Sea. Curr. Biol. *18*, 1349–1354.
7. Hughes, T.P. (1994). Catastrophes, phase shifts, and large-scale degradation of a Caribbean coral reef. Science *265*, 1547–1551.
8. Hughes, D.J., Alderdice, R., Cooney, C., Kühl, M., Pernice, M., Voolstra, C.R., and Suggett, D.J. (2020). Coral reef survival under accelerating ocean deoxygenation. Nat. Clim. Change *10*, 296–307.
9. Knowlton, N., Grottoli, A.G., Kleypas, J.A., Obura, D., Corcoran, E., de Goeij, J.M., Felis, T., Harding, S.P., Mayfield, A.B., Miller, M.W., et al. (2021). Rebuilding Coral Reefs: A Decadal Grand Challenge (International Coral Reef Society).
10. Hughes, T.P., Kerry, J.T., Álvarez-Noriega, M., Álvarez-Romero, J.G., Anderson, K.D., Baird, A.H., Babcock, R.C., Beger, M., Bellwood, D.R., Berkelmans, R., et al. (2017). Global warming and recurrent mass bleaching of corals. Nature *543*, 373–377.
11. Hoegh-Guldberg, O., and Jones, R. (1999). Photoinhibition and photoprotection in symbiotic dinoflagellates from reef-building corals. Mar. Ecol. Prog. Ser. *183*, 73–86.
12. De'ath, G., Fabricius, K.E., Sweatman, H., and Puotinen, M. (2012). The 27-year decline of coral cover on the Great Barrier Reef and its causes. Proc. Natl. Acad. Sci. USA *109*, 17995–17999.
13. Putnam, H.M., Barott, K.L., Ainsworth, T.D., and Gates, R.D. (2017). The vulnerability and resilience of reef-building corals. Curr. Biol. *27*, R528–R540.
14. Muscatine, L. (1973). Nutrition of Corals. In Biology and Geology of Coral Reefs, , O.A. Jones, and R. Endean, eds. (Academic Press), pp. 77–115.
15. Muller, E.B., Kooijman, S.A.L.M., Edmunds, P.J., Doyle, F.J., and Nisbet, R.M. (2009). Dynamic energy budgets in syntrophic symbiotic relationships between heterotrophic hosts and photoautotrophic symbionts. J. Theor. Biol. *259*, 44–57.

Please cite this article in press as: Pacherres et al., Ciliary flows in corals ventilate target areas of high photosynthetic oxygen production, Current Biology (2022), https://doi.org/10.1016/j.cub.2022.07.071

16. Muscatine, L., Ferrier-Pagès, C., Blackburn, A., Gates, R.D., Baghdasarian, G., and Allemand, D. (1998). Cell-specific density of symbiotic dinoflagellates in tropical anthozoans. Coral Reefs *17*, 329–337.
17. Wangpraseurt, D., Wentzel, C., Jacques, S.L., Wagner, M., and Kühl, M. (2017). *In vivo* imaging of coral tissue and skeleton with optical coherence tomography. J. R. Soc. Interface *14*, 20161003.
18. Laissue, P.P., Roberson, L., Gu, Y., Qian, C., and Smith, D.J. (2020). Long-term imaging of the photosensitive, reef-building coral *Acropora muricata* using light-sheet illumination. Sci. Rep. *10*, 10369.
19. Dubinsky, Z., Falkowski, P.G., Porter, J.W., Muscatine, L., and Smith, D.C. (1984). Absorption and utilization of radiant energy by light- and shade-adapted colonies of the hermatypic coral *Stylophora pistillata*. Proc. R. Soc. Lond. B *222*, 203–214.
20. Falkowski, P.G., and Dubinsky, Z. (1981). Light-shade adaptation of *Stylophora pistillata*, a hermatypic coral from the Gulf of Eilat. Nature *289*, 172–174.
21. Wangpraseurt, D., Larkum, A.W., Ralph, P.J., and Kühl, M. (2012). Light gradients and optical microniches in coral tissues. Front. Microbiol. *3*, 316.
22. Al-Horani, F.A., Al-Moghrabi, S.M., and de Beer, D. (2003). The mechanism of calcification and its relation to photosynthesis and respiration in the scleractinian coral *Galaxea fascicularis*. Mar. Biol. *142*, 419–426.
23. Shashar, N., Cohen, Y., and Loya, Y. (1993). Extreme diel fluctuations of oxygen in diffusive boundary layers surrounding stony corals. Biol. Bull. *185*, 455–461.
24. Kühl, M., Cohen, Y., Dalsgaard, T., Jørgensen, B.B., and Revsbech, N.P. (1995). Microenvironment and photosynthesis of zooxanthellae in scleractinian corals studied with microsensors for O_2, pH and light. Mar. Ecol. Prog. Ser. *117*, 159–172.
25. Weis, V.M., Smith, G.J., and Muscatine, L. (1989). A "CO_2 supply" mechanism in zooxanthellate cnidarians: role of carbonic anhydrase. Mar. Biol. *100*, 195–202.
26. Nakamura, T., van Woesik, R., and Yamasaki, H. (2005). Photoinhibition of photosynthesis is reduced by water flow in the reef-building coral *Acropora digitifera*. Mar. Ecol. Prog. Ser. *301*, 109–118.
27. van Woesik, R., Irikawa, A., Anzai, R., and Nakamura, T. (2012). Effects of coral colony morphologies on mass transfer and susceptibility to thermal stress. Coral Reefs *31*, 633–639.
28. de Beer, D., Kühl, M., Stambler, N., and Vaki, L. (2000). A microsensor study of light enhanced Ca^{2+} uptake and photosynthesis in the reef-building hermatypic coral *Favia* sp. Mar. Ecol. Prog. Ser. *194*, 75–85.
29. Al-Horani, F.A., Ferdelman, T., Al-Moghrabi, S.M., and de Beer, D. (2005). Spatial distribution of calcification and photosynthesis in the scleractinian coral *Galaxea fascicularis*. Coral Reefs *24*, 173–180.
30. Nakamura, T., Yamasaki, H., and van Woesik, R. (2003). Water flow facilitates recovery from bleaching in the coral *Stylophora pistillata*. Mar. Ecol. Prog. Ser. *256*, 287–291.
31. Fifer, J., Bentlage, B., Lemer, S., Fujimura, A.G., Sweet, M., and Raymundo, L.J. (2021). Going with the flow: how corals in high-flow environments can beat the heat. Mol. Ecol. *30*, 2009–2024.
32. Mass, T., Genin, A., Shavit, U., Grinstein, M., and Tchernov, D. (2010). Flow enhances photosynthesis in marine benthic autotrophs by increasing the efflux of oxygen from the organism to the water. Proc. Natl. Acad. Sci. USA *107*, 2527–2531.
33. Pacherres, C.O., Ahmerkamp, S., Schmidt-Grieb, G.M., Holtappels, M., and Richter, C. (2020). Ciliary vortex flows and oxygen dynamics in the coral boundary layer. Sci. Rep. *10*, 7541.
34. Shapiro, O.H., Fernandez, V.I., Garren, M., Guasto, J.S., Debaillon-Vesque, F.P., Kramarsky-Winter, E., Vardi, A., and Stocker, R. (2014). Vortical ciliary flows actively enhance mass transport in reef corals. Proc. Natl. Acad. Sci. USA *111*, 13391–13396.
35. Lesser, M.P., and Shick, J.M. (1989). Effects of irradiance and ultraviolet radiation on photoadaptation in the zooxanthellae of *Aiptasia pallida* primary production, photoinhibition, and enzymic defenses against oxygen toxicity. Mar. Biol. *102*, 243–255.
36. Baird, M.E., Mongin, M., Rizwi, F., Bay, L.K., Cantin, N.E., Soja-Woźniak, M., and Skerratt, J. (2018). A mechanistic model of coral bleaching due to temperature-mediated light-driven reactive oxygen build-up in zooxanthellae. Ecol. Modell. *386*, 20–37.
37. Lesser, M.P. (1996). Elevated temperatures and ultraviolet radiation cause oxidative stress and inhibit photosynthesis in ymbiotic dinoflagellates. Limnol. Oceanogr. *41*, 271–283.
38. Crawley, A., Kline, D.I., Dunn, S., Anthony, K., and Dove, S. (2010). The effect of ocean acidification on symbiont photorespiration and productivity in *Acropora formosa*. Glob. Change Biol. *16*, 851–863.
39. Shick, J.M. (1990). Diffusion limitation and hyperoxic enhancement of oxygen consumption in zooxanthellate sea anemones, zoanthids, and corals. Biol. Bull. *179*, 148–158.
40. Lesser, M.P. (1997). Oxidative stress causes coral bleaching during exposure to elevated temperatures. Coral Reefs *16*, 187–192.
41. Lesser, M.P., Stochaj, W.R., Tapley, D.W., and Shick, J.M. (1990). Bleaching in coral reef anthozoans: effects of irradiance, ultraviolet radiation, and temperature on the activities of protective enzymes against active oxygen. Coral Reefs *8*, 225–232.
42. Yakovleva, I.M., Baird, A.H., Yamamoto, H.H., Bhagooli, R., Nonaka, M., and Hidaka, M. (2009). Algal symbionts increase oxidative damage and death in coral larvae at high temperatures. Mar. Ecol. Prog. Ser. *378*, 105–112.
43. Joyce, K.E., and Phinn, S.R. (2003). Hyperspectral analysis of chlorophyll content and photosynthetic capacity of coral reef substrates. Limnol. Oceanogr. *48*, 489–496.
44. Pacherres, C.O., Schmidt, G.M., and Richter, C. (2013). Autotrophic and heterotrophic responses of the coral *Porites lutea* to large amplitude internal waves. J. Exp. Biol. *216*, 4365–4374.
45. Lasker, H.R. (1979). Light dependent activity patterns among reef corals: *Montastrea cavernosa*. Biol. Bull. *156*, 196–211.
46. Sebens, K.P., and DeRiemer, K. (1977). Diel cycles of expansion and contraction in coral reef anthozoans. Mar. Biol. *43*, 247–256.
47. Spicer, G.L.C., Eid, A., Wangpraseurt, D., Swain, T.D., Winkelmann, J.A., Yi, J., Kühl, M., Marcelino, L.A., and Backman, V. (2019). Measuring light scattering and absorption in corals with inverse spectroscopic optical coherence tomography (ISOCT): a new tool for non-invasive monitoring. Sci. Rep. *9*, 14148.
48. Liu, C., Cheng, S.H., and Lin, S. (2020). Illuminating the dark depths inside coral. Cell. Microbiol. *22*, e13122.
49. Koren, K., Jakobsen, S.L., and Kühl, M. (2016). In-vivo imaging of O_2 dynamics on coral surfaces spray-painted with sensor nanoparticles. Sens. Actuators B *237*, 1095–1101.
50. Ahmerkamp, S., Jalaluddin, F.M., Cui, Y., Brumley, D.R., Pacherres, C.O., Berg, J.S., Stocker, R., Kuypers, M.M.M., Koren, K., and Behrendt, L. (2022). Simultaneous visualization of flow fields and oxygen concentrations to unravel transport and metabolic processes in biological systems. Cell Rep. Methods *2*, 100216.
51. Sforza, E., Pastore, M., Franke, S.M., and Barbera, E. (2020). Modeling the oxygen inhibition in microalgae: an experimental approach based on photorespirometry. New Biotechnol. *59*, 26–32.
52. Loya, Y., Sakai, K., Yamazato, K., Nakano, Y., Sambali, H., and van Woesik, R. (2001). Coral bleaching: the winners and the losers. Ecol. Lett. *4*, 122–131.
53. Finelli, C.M., Helmuth, B.S.T., Pentcheff, N.D., and Wethey, D.S. (2006). Water flow influences oxygen transport and photosynthetic efficiency in corals. Coral Reefs *25*, 47–57.
54. Nielsen, D.A., Petrou, K., and Gates, R.D. (2018). Coral bleaching from a single cell perspective. ISME J. *12*, 1558–1567.
55. Jordan, D.B., and Ogren, W.L. (1981). Species variation in the specificity of ribulose biphosphate carboxylase/oxygenase. Nature *291*, 513–515.
56. Roberty, S., Bailleul, B., Berne, N., Franck, F., and Cardol, P. (2014). PSI Mehler reaction is the main alternative photosynthetic electron pathway

Please cite this article in press as: Pacherres et al., Ciliary flows in corals ventilate target areas of high photosynthetic oxygen production, Current Biology (2022), https://doi.org/10.1016/j.cub.2022.07.071

in *Symbiodinium* sp., symbiotic dinoflagellates of cnidarians. New Phytol. *204*, 81–91.

57. Brown, B., Dunne, R., Goodson, M., and Douglas, A. (2002). Experience shapes the susceptibility of a reef coral to bleaching. Coral Reefs *21*, 119–126.
58. Safaie, A., Silbiger, N.J., McClanahan, T.R., Pawlak, G., Barshis, D.J., Hench, J.L., Rogers, J.S., Williams, G.J., and Davis, K.A. (2018). High frequency temperature variability reduces the risk of coral bleaching. Nat. Commun. *9*, 1671.
59. Cunning, R., Ritson-Williams, R., and Gates, R.D. (2016). Patterns of bleaching and recovery of *Montipora capitata* in Kāne'ohe Bay, Hawai'i, USA. Mar. Ecol. Prog. Ser. *551*, 131–139.
60. Al-Horani, F.A., Al-Moghrabi, S.M., and de Beer, D. (2003). Microsensor study of photosynthesis and calcification in the scleractinian coral, *Galaxea fascicularis*: active internal carbon cycle. J. Exp. Mar. Biol. Ecol. *288*, 1–15.
61. Agostini, S., Suzuki, Y., Higuchi, T., Casareto, B.E., Yoshinaga, K., Nakano, Y., and Fujimura, H. (2012). Biological and chemical characteristics of the coral gastric cavity. Coral Reefs *31*, 147–156.
62. Hoegh-Guldberg, O., Mumby, P.J., Hooten, A.J., Steneck, R.S., Greenfield, P., Gomez, E., Harvell, C.D., Sale, P.F., Edwards, A.J., Caldeira, K., et al. (2007). Coral reefs under rapid climate change and ocean acidification. Science *318*, 1737–1742.
63. Comeau, S., Cornwall, C.E., Pupier, C.A., DeCarlo, T.M., Alessi, C., Trehern, R., and McCulloch, M.T. (2019). Flow-driven micro-scale pH variability affects the physiology of corals and coralline algae under ocean acidification. Sci. Rep. *9*, 12829.
64. Chan, N.C.S., Wangpraseurt, D., Kühl, M., and Connolly, S.R. (2016). Flow and coral morphology control coral surface ph: implications for the effects of ocean acidification. Front. Mar. Sci. *3*, 10.
65. McCulloch, M., Falter, J., Trotter, J., and Montagna, P. (2012). Coral resilience to ocean acidification and global warming through pH up-regulation. Nat. Clim. Change *2*, 623–627.
66. McCulloch, M.T., D'Olivo, J.P., Falter, J., Holcomb, M., and Trotter, J.A. (2017). Coral calcification in a changing world and the interactive dynamics of pH and DIC upregulation. Nat. Commun. *8*, 15686.
67. Ainsworth, T.D., Fordyce, A.J., and Camp, E.F. (2017). The other microeukaryotes of the coral reef microbiome. Trends Microbiol. *25*, 980–991.
68. Webster, N.S., and Reusch, T.B.H. (2017). Microbial contributions to the persistence of coral reefs. ISME J. *11*, 2167–2174.
69. Bourne, D.G., Morrow, K.M., and Webster, N.S. (2016). Insights into the coral microbiome: underpinning the health and resilience of reef ecosystems. Annu. Rev. Microbiol. *70*, 317–340.
70. Sweet, M.J., and Séré, M.G. (2016). Ciliate communities consistently associated with coral diseases. J. Sea Res. *113*, 119–131.
71. Gerardo, N.M. (2013). The give and take of host-microbe symbioses. Cell Host Microbe *14*, 1–3.
72. Wegley, L., Edwards, R., Rodriguez-Brito, B., Liu, H., and Rohwer, F. (2007). Metagenomic analysis of the microbial community associated with the coral *Porites astreoides*. Environ. Microbiol. *9*, 2707–2719.
73. van Oppen, M.J.H., Leong, J.-A., and Gates, R.D. (2009). Coral–virus interactions: a double-edged sword? Symbiosis *47*, 1–8.
74. Klein, R., Pätzold, J., Wefer, G., and Loya, Y. (1993). Depth-related timing of density band formation in Porites spp. corals from the Red Sea inferred from X-ray chronology and stable isotope composition. Mar. Ecol. Prog. Ser. *97*, 99–104.
75. Veron, J.E.N. (2000). Corals of the World (Australian Institute of Marine Science).
76. Wall, M., Putchim, L., Schmidt, G.M., Jantzen, C., Khokiattiwong, S., and Richter, C. (2015). Large-amplitude internal waves benefit corals during thermal stress. Proc. Biol. Sci. *282*, 20140650.
77. Hackerott, S., Martell, H.A., and Eirin-Lopez, J.M. (2021). Coral environmental memory: causes, mechanisms, and consequences for future reefs. Trends Ecol. Evol. *36*, 1011–1023.
78. Koren, K., Brodersen, K.E., Jakobsen, S.L., and Kühl, M. (2015). Optical sensor nanoparticles in artificial sediments – a new tool to visualize O_2 dynamics around the rhizome and roots of seagrasses. Environ. Sci. Technol. *49*, 2286–2292.
79. Willert, C., Stasicki, B., Klinner, J., and Moessner, S. (2010). Pulsed operation of high-power light emitting diodes for imaging flow velocimetry. Meas. Sci. Technol. *21*, 075402.
80. Bartzke, G., Siemann, L., Büssing, R., Nardone, P., Koll, K., Hebbeln, D., and Huhn, K. (2021). Investigating the prevailing hydrodynamics around a cold-water coral colony using a physical and a numerical approach. Front. Mar. Sci. *8*, 1375.

Please cite this article in press as: Pacherres et al., Ciliary flows in corals ventilate target areas of high photosynthetic oxygen production, Current Biology (2022), https://doi.org/10.1016/j.cub.2022.07.071

STAR★METHODS

KEY RESOURCES TABLE

REAGENT or RESOURCE	SOURCE	IDENTIFIER
Experimental models: Organisms/strains		
Porites lutea	Alfred Wegener Institute, Claudio Richter, Pacherres et al.[44]	https://doi.org/10.1242/jeb.085548
Software and algorithms		
sensPIV processing	Ahmerkamp at al.[50]	https://doi.org/10.1016/j.crmeth.2022.100216
Matlab 2018b	Mathworks	https://de.mathworks.com
Comsol Multiphysics v5.6	Comsol	https://www.comsol.com
Python	Phyton	https://www.python.org/
SensorTrace-PRO	Unisense	N/A
Micro-hyperspectral algorithm	This paper	https://doi.org/10.6084/m9.figshare.20347899.v1
Other		
RGB cmos camera	FLIR	GS3-U3-51S5C-C
Lens array	Optem Fusion	N/A
LED pulsing system	iLA_5150	LPS3
Gear Pump	Ismatec	ISM901B
Long-pass filter	Midopt	LP515
Polyester Optical Filters	Lee Felters	010 Medium Yellow
Temperature sensor	PyroScience	Pt100
Oxygen microsensor	Unisense	OX-10
Micromanipulator	Unisense	N/A
Fiber optic lamp	Schott	1500
Lens for hyperspectral system	Optem Fusion	N/A
Hyperspectral camera	FLIR	Blackfly
Micromanipulator	PyroScience	N/A

RESOURCE AVAILABILITY

Lead contact

Further information and requests for resources should be directed and will be fulfilled by the lead contact, Cesar O. Pacherres (cesar.pacherres@bio.ku.dk).

Materials availability

This study did not generate new unique reagents.

Data and code availability

- All data reported in this paper will be shared by the lead contact upon request.
- All original code is publicly available as of the date of publication. DOI is listed in the key resources table.
- Any additional information required to reanalyze the data reported in this paper is available from the lead contact upon request.

EXPERIMENTAL MODEL AND SUBJECT DETAILS

Colonies of the massive coral *Porites lutea*, reared at the aquaria facilities of the Alfred Wegener Institute (AWI) were used as fragment source. They were kept in artificial seawater (salinity 32.25 ± 2.89) (Dupla Marine Premium Reef Salt Natural Balance) under conditions mimicking those found at the depth of their origin (15 m), i.e. 25.2 ± 0.17 °C, a 12-h light-dark cycle, light intensities between 75 and 80 μmol quanta m^{-2} s^{-1} (LI-COR LI-192, USA) (see also Figure S4) and a pH of 7.9 ± 0.11 (YSI, USA) (see also Table S3 for extended parameters). Food was provided in the form of freshly hatched *Artemia* nauplii every second day. Before the start of the experiments,

Please cite this article in press as: Pacherres et al., Ciliary flows in corals ventilate target areas of high photosynthetic oxygen production, Current Biology (2022), https://doi.org/10.1016/j.cub.2022.07.071

CellPress
OPEN ACCESS

small fragments (2 cm long, 2 cm wide) bearing 60 to 80 polyps were cut out from 4 of the source colonies and allowed to heal for at least one month in the same culturing tanks their original colonies were kept. Survival of the fragments was >90%.

Porites was chosen as a model organism as it occurs over a wide depth range from surface down to 50 m[74] being an important reef building coral along different regions.[75] Moreover, it has been shown to experience bleaching at 15 m[76] making it an ideal subject to test our hypotheses.

METHOD DETAILS

Experimental set-up

For all experiments, the light-sheet-microscopy based flow chamber set-up was used, as in Pacherres et al.[33] (Figures 1A and 2A). The coral fragment was placed in the chamber filled with filtered artificial seawater (FASW) (0.2 μm pore size) from the coral's culturing tank. There, it was allowed to acclimate to the chamber conditions for at least an hour under dark and low flow conditions (300 μm s^{-1}) before experiments started. Temperature of the water inside the chamber was monitored every 30 seconds (Pt100 sensor, PyroScience, Germany). For all experiments, temperature was kept constant at 25 °C ± 0.5. Flow rate inside the chamber was modulated using a water pump (REGLO Z, ISMATEC, Germany). Experiments were conducted at 2 flow rates: 300 μm s^{-1} and 1500 μm s^{-1} measured at 2 mm above the coral tissue. In the case of experiments requiring a light source, a fiber optic lamp (Schott 1500, USA) was used in order to maintain constant illumination of 180 μmol quanta m^{-2} s^{-1} (LI-COR LI-192, USA). In order to standardize respiratory differences due to digestion, all experiments were performed after 2 days of starvation.

Experiments under dark conditions were performed after one hour of acclimating the coral to the chamber. After those images were taken, light was turned on for 5 minutes, to allow the coral to build a representative concentration boundary layer, before capturing the images for the light experiments.

Experiments with arrested cilia were initially planned by adding sodium orthovanadate. However, we were surprised to find that some corals adapted to the addition of the chemical as cilia activity ceased to fully arrest, suggesting an environmental memory.[77] We therefore decided against continuing with sodium orthovanadate to avoid introducing dose-response and other inconclusive treatment effects into this study. The effect of arrested cilia activity on the oxygen dynamics of the coral DBL has been shown in previous studies.[33,34]

Hyperspectral imaging

Chl*a* concentrations of Symbiodiniaceae inside the tissue of the coral colony were obtained using hyperspectral line-scanning. For that, hyperspectral imaging optics (Wasatch, USA) were used. Briefly, a line is recorded through a long-distance microscope lens (Optem Fusion) and directed through a diffraction grid. The resulting light spectrum is aligned with a camera CCD chip (FLIR, blackfly, Canada) along a pixel row of 1288 px. in the visible light range, this results in a spectral resolution of approx. 1 nm. Using a micromanipulator (PyroScience, Germany) the camera system was slowly moved parallel to the coral surface at a speed of 50 μm s^{-1} to the focused line along the coral fragment while continuously recording images with an exposure time of 400 ms. This resulted in a 3D tensor or hypercube, i.e. each pixel of the image consists of a spectrum ranging from 400 – 700 nm. Horizontal and vertical resolution was 42 and 6 μm per px, respectively. The set-up was controlled using serial-interfaces and the Spinnaker Software Development Kit (FLIR Spinnaker SDK) through an in-house developed Python script (Python Software Foundation). The raw images were processed using Matlab (2018b).

Chl*a* pigments reflect green light and absorb light in the blue-violet and orange-red range with peaks at 450 – 475 nm and around 650 – 680 nm, respectively. In our hyperspectral line-scanning set-up, reflectance spectra were measured, implying that low spectral intensities correspond to a high absorbance and, conversely, high spectral intensities correspond to low absorbance. Therefore, to estimate the absorbance spectra induced by the Chl*a*, we subtracted the integrated wavelengths 650 nm – 660 nm from the reference light spectrum. To compensate for lower light intensity and 3D structures at the surface of the coral, we normalized the resulting absorbance spectrum by Chl*a* unaffected wavelengths between 550 nm and 560 nm. Therefore, the resulting normalized absorbance value indicates the amount of orange-red light that is absorbed from the incident light, which depends on the amount of Chl*a* in the tissue of the coral.

During the experimental procedure, the coral fragment was placed in the flow-chamber (Figure 1A) and illuminated using a homogenous white light (Schott 1500, USA), intensity reached 160 μmol quanta m^{-2} s^{-1} (LI-COR LI-192, USA). The chamber was placed on top of a white surface, which later served as reference.

SensPIV measurements

In order to identify the relative influence of cilia activity on the 2D structure of the O_2 DBL at the coral surface, O_2 distributions were compared under light and dark conditions (180 and 0 μmol quanta m^{-2} s^{-1} respectively). To resolve the O_2 and flow field around the coral fragment, we used O_2 sensitive nanoparticles,[78] which have proven ideal for mapping O_2 concentrations at relevant scales.[50] The stock solution contained 2 mg mL^{-1} which was further diluted by a factor of 200. Illumination was achieved using a LED pulsing system (LPS3, iLA_5150, Germany) connected to LED light sheet optics similar to the one described by Willert et al.[79] The light sheet was approx. 1 mm thick and intensity reached 4500 μmol quanta m^{-2} s^{-1} (LI-COR LI-192, USA) at a wavelength of around 468 nm. For each experiment one hundred images were captured using a Grasshopper3 camera (FLIR, USA) recording at 20 frames per second (fps) with an exposure time of 50 ms. A long distance custom-made microscope lens (based on the Optem FUSION system, Germany) with a yellow-orange long-pass filter (515 nm, LP515, Midopt, USA) was used for all experiments. To avoid photoinhibition of the symbionts from the intense illumination, light exposure was limited to 5 s for each experiment and LED light was only active

Please cite this article in press as: Pacherres et al., Ciliary flows in corals ventilate target areas of high photosynthetic oxygen production, Current Biology (2022), https://doi.org/10.1016/j.cub.2022.07.071

during 50 ms illumination of the camera chip. The recorded images were post-processed using custom-built Matlab (MathWorks, R2018b) algorithms to obtain the O_2 concentration signal and a map of the particle movement inside the chamber.

Nanoparticle readings were later compared and calibrated with O_2 profiles, performed before each experiment, using an electrochemical sensor of 10 μm tip diameter (Unisense, Denmark). The profile was recorded 3 min before the images were captured. Values were recorded using the SensorTrace-PRO software (Unisense, Denmark). For each experiment, microelectrodes were 2-point calibrated in O_2-free (bubbling pre-filtered seawater with N_2 gas for 10 min) and air-saturated FASW of known salinity and temperature.[24] The tip of the sensor was carefully placed at the surface of the coral. A micromanipulator (Unisense, Denmark) was programmed to move the sensor up in 20 μm steps. The range of the vertical profile was 1000 μm. At each step, dissolved O_2 was measured one time with a sampling interval of 2 s.

To directly relate the O_2 production of the coral colony with the Chl*a* concentration inside the coral tissue we carefully pinpoint the area of the coral observed through the camera and later extracted the Chl*a* concentrations from the same area out of the hyperspectral images.

QUANTIFICATION AND STATISTICAL ANALYSIS

Model formulation

The cilia beating of corals generates a complex flow pattern, which is reproduced using numerical simulations which were performed in Comsol (Comsol Multiphysics, V5.6). The flow field is given by the Stokes equations:

$$0 = -\nabla p + \mu \nabla^2 \boldsymbol{u} \quad \text{(Equation 1)}$$

Where $\boldsymbol{u}$ is the velocity vector, p the pressure, μ dynamic viscosity and ∇ the gradient-operator. The continuity equation for incompressible fluids reads:

$$\nabla \cdot \boldsymbol{u} = 0 \quad \text{(Equation 2)}$$

The O_2 distribution was calculated solving the stationary advection-diffusion equations:

$$0 = D\nabla^2 C - \boldsymbol{u} \cdot \nabla C + R_H \quad \text{(Equation 3)}$$

R_H is the volumetric O_2 production rate (see below), D is the diffusion coefficient for O_2 in sea water at 20° C: 2.1 10^{-9} m^2 s^{-1}. According to the model proposed by Shapiro,[34] the cilia-induced currents were simulated assuming oscillating horizontal velocity components at the coral surface (slip boundary condition):

$$u_x = c_{vel} \cdot \sin\left(\frac{2\pi}{\delta} x\right) \quad \text{(Equation 4)}$$

where x is the horizontal distance, c_{vel} the maximum ciliate beating velocity and δ is the characteristic length scale of the vortices, see text for values and explanation. Volumetric rates of O_2 production in the tissue were simulated based on the assumption that the clustering of chlorophyll a at certain areas of the tissue follows a sinus curve:

$$R_H = R_C \left(1 + \sin\left(\frac{2\pi}{\delta} x + m\pi\right)\right) \quad \text{(Equation 5)}$$

Where R_C is the production rate, m is the parameter for the relative phase shift. The mathematical model allowed us to simulate O_2 concentrations inside the DBL and in the tissue in the presence of a heterogeneous O_2 production rate by the coral.

Limitations of the model and topography effects

We applied a simplified 2D transport-reaction model in order to investigate the effect of the ciliary flow on the O_2 concentration inside the tissue and within the coral boundary layer. The model approach does not consider 3D effects or changes in the topography of the coral, which might become substantial when investigating the turbulent flow field along an entire coral colony see for example Bartzke et al.[80] However, on the scales of the investigated coral fragments, the topographical features where an order of magnitude smaller (21 – 123 μm) than the observed vortices (typically around 1 mm) and were not a substantial factor within the experiments. It remains a task for future studies to investigate how O_2 is re-distributed along an entire coral colony and how topography and ciliary flow act in tandem for coral ventilation.

Further, in the modelling approach we investigated the effect of the ciliary flow by comparing the tissue volume below and above a specific O_2-threshold of 300 μmol L^{-1} (Figure S5). This O_2-threshold was inferred from an experiment in which a microsensor was placed directly above the coral tissue and the light intensity was increased until O_2 production was affected (see Figure S5). However, to test the sensitivity of the obtained model results, we tested varying thresholds between 200 μmol L^{-1} and 400 μmol L^{-1}. Overall, the pattern of maxima and minima along the different phase shifts persisted. Only the difference between the maximum and minimum varied between 6-19 % (compared to 18% for 300 μmol L^{-1}, see Table S2).